Inorganic Chemistry

pubs.acs.org/IC

Communication

Photoinduced Low-Spin → High-Spin Mechanism of an Octahedral Fe(II) Complex Revealed by Synergistic Spin-Vibronic Dynamics

Mátyás Pápai*

Cite This: *Inorg. Chem.* 2021, 60, 13950−13954

Read Online

ACCESS | Metrics & More | Article Recommendations | Supporting Information

ABSTRACT: The Fe(II) low-spin (LS; $^1A_{1g}$, $t_{2g}^6e_g^0$) → high-spin (HS; $^5T_{2g}$, $t_{2g}^4e_g^2$) light-induced excited spin state trapping (LIESST) mechanism solely involving metal-centered states is revealed by synergistic spin-vibronic dynamics simulations. For the octahedral $[Fe(NCH)_6]^{2+}$ complex, we identify an initial ∼100 fs $^1T_{1g} \rightarrow {}^3T_{2g}$ intersystem crossing, controlled by vibronic coupling to antisymmetric Fe−N stretching motion. Subsequently, population branching into $^3T_{1g}$, $^5T_{2g}$ (HS), and $^1A_{1g}$ (LS) is observed on a subpicosecond time scale, with the dynamics dominated by coherent Fe−N breathing wavepackets. These findings are consistent with ultrafast experiments, methodologically establish a new state of the art, and will give a strong impetus for further intriguing dynamical studies on LS → HS photoswitching.

Photoinduced low-spin (LS) → high-spin (HS) transition in transition-metal complexes, known as light-induced excited spin state trapping (LIESST), has attracted great interest since its discovery in 1984.[1] LIESST is an intriguing phenomenon both from the point of view of the fundamentals of excited-state processes and revolutionary applicational areas, such as molecular data storage.[2] It is known that the LS-to-HS transition can also be triggered by varying the temperature, pressure, and magnetic field;[3] in fact, the first discovery of these so-called spin-crossover (SCO) complexes is dated way back to 1931.[4]

In the past two decades, the LIESST mechanism has been a very "hot" research topic; this is motivated by the fact that the gained knowledge may allow control of excited-state pathways and thus can lead to the design of improved functional molecules and technologies. In the case of switchable hexacoordinated complexes with a $Fe^{II}N_6$ core, which by far dominate the known LIESST-exhibiting systems, irradiation of light converts the singlet ground state [$^1A_{1g}$(LS), $t_{2g}^6e_g^0$] into a quintet metastable state [$^5T_{2g}$(HS), $t_{2g}^4e_g^2$]; thus, a $\Delta S = 2$ net change of the spin momentum occurs. The LIESST mechanism was first investigated in 1991 by Hauser[5] for the 1-propyltetrazole $[Fe(ptz)_6](BF_4)_2$ pseudooctahedral SCO Fe(II) complex, promoted to the lowest singlet metal-centered (MC) state. Utilizing UV/vis/near-IR absorption spectroscopy, he identified a triplet intermediate state, which at 10 K decays via branching into a quintet metastable state [$^5T_{2g}$(HS), 75%] and the ground state [$^1A_{1g}$(LS), 25%], occurring via intersystem crossing (ISC), as illustrated in Figure 1. More recently, for the Zn-doped crystal $[Zn_{0.9}Fe_{0.1}(ptz)_6](BF_4)_2$, probed at 125 K by time-resolved absorption spectroscopy, Hauser and co-workers identified the upper triplet $^3T_{2g}$ as the intermediate state, which is formed from $^1T_{1g}$ in <150 fs and decays into the $^5T_{2g}$ HS state in 1.2 ps.[6] The HS state is metastable at low temperatures (T < 50 K), and its lifetime is determined by quantum-mechanical tunneling.

Despite these valuable mechanistic insights, several unknowns remain, in most cases, because of the ambiguities in the interpretation of the experimental data. An excellent example is the more complicated case of $[Fe(bipy)_3]^{2+}$ (bipy = 2,2′-bipyridine), a LS Fe(II) complex, which became the LS ↔ HS photoswitching prototype for time-resolved investigations. $[Fe(bipy)_3]^{2+}$ is converted to the HS state in <100 fs, initiated

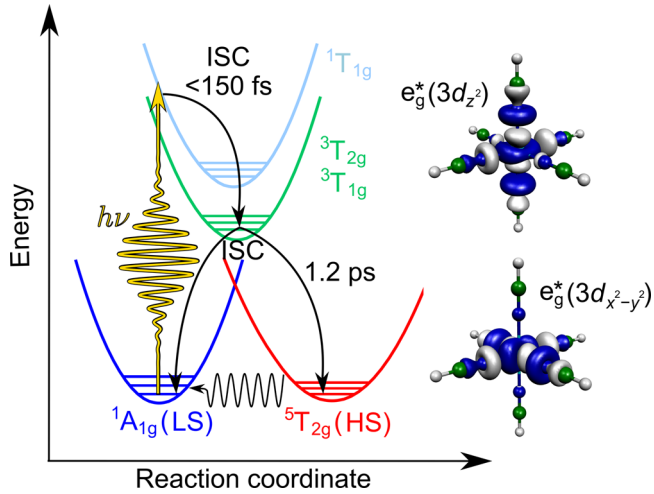

Figure 1. Schematic mechanistic picture of the LIESST effect in the case of excitation into the lowest ^{1}MC ($^1T_{1g}$) state by 530 nm light. The wavy arrow illustrates the low-temperature HS → LS relaxation by tunneling. The excited-state lifetimes are taken for $[Zn_{0.9}Fe_{0.1}(ptz)_6](BF_4)_2$ from ref 6. The electronic state labels are consistent with O_h point group symmetry. Also shown are the e_g* antibonding orbitals of the complex investigated in the present work, $[Fe(NCH)_6]^{2+}$, which are populated in the excited states.

Received: June 17, 2021
Published: September 9, 2021

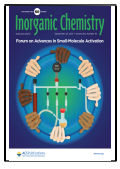

https://doi.org/10.1021/acs.inorgchem.1c01838
Inorg. Chem. 2021, 60, 13950−13954

by irradiation into the optically active singlet metal-to-ligand charge-transfer (MLCT) band. This <100 fs time scale and the HS lifetime (ca. 650 ps in aqueous solution) are consistent for various experimental studies, but it is strongly debated how the HS state is populated.[7−9] A final consensus is yet to be established; in order to achieve this goal, theory, which has the potential to complement and support time-resolved experiments, has a crucial role. However, the computational state of the art for light-induced singlet-to-quintet transitions has so far been limited to analysis of the static potential energy surfaces (PESs)[10]/couplings[11] and estimation of the excited-state lifetimes by Fermi's golden rule.[12,13] Albeit often useful, these approaches face severe shortcomings when it comes to fast electronic relaxation such as LIESST, with a time scale comparable to that of nuclear motion. In fact, this nuclear−electronic coupling, leading to a dynamic mixing of the electronic states, is among the main sources for the complexity of the obtained time-resolved experimental data, which theory is intended to alleviate.

In this Communication, we present the first theoretical dynamics study on LS → HS photoswitching with excitation into ^{1}MC states ($^1T_{1g}$, $[Fe(ptz)_6]^{2+}$ prototype; Figure 1). In order to achieve feasibility at a high computational level, we investigate the excited-state dynamics of $[Fe(NCH)_6]^{2+}$, a well-established model[14−17] for metastable Fe(II)-based SCO systems. Its validity, with a special emphasis on LIESST, is discussed in the Supporting Information (SI). Employing a synergistic spin-vibronic approach,[18,19] we achieve an invaluable mechanistic understanding, whose adequacy is assessed and confirmed by its consistency with the above-discussed experiments.

Herein, we employ a synergistic approach, which exploits the complementary character of trajectory surface hopping (TSH; full dimensionality) and quantum dynamics (QD; fully quantum description). We utilize full-dimensional TSH on potentials computed on-the-fly to select the dominant nuclear degrees of freedom and QD on high-level ab initio (CASPT2) precomputed surfaces along the selected modes for the accurate simulation of LIESST excited-state dynamics. A brief methodological description is provided in the Computational Methods section, with details given in the SI.

Figure 2 presents the normal-mode activity of the vibrational motion, obtained from the excited-state TSH trajectories. As is clear from the figure, three modes, ν_{13}, ν_{14}, and ν_{15}, dominate the excited-state nuclear motion. As shown in Figure 3, all three modes have Fe−N stretching character, but while the 2-fold-degenerate ν_{13} and ν_{14} modes are antisymmetric, ν_{15} is a totally symmetric (breathing) mode. These three Fe−N stretching modes are in excellent agreement with the natural choice of coordinates upon the occupation of e_g* antibonding orbitals, shown in Figure 1, in MC excited states.

Figure 4 shows the PESs along modes ν_{15} and ν_{14}; the PESs along ν_{13} are shown in Figure S7. While the ν_{15} breathing mode is crucial to connect the LS ($^1A_{1g}$) and HS ($^5T_{2g}$) states (Figure 4a), it maintains the octahedral symmetry and does not allow the different singlet and triplet MC components to cross. The reason for this is that, in the singlet and triplet excited states, a single e_g* orbital is populated, which activates antisymmetric Fe−N stretching modes, while the ν_{15} breathing mode is totally symmetric. Indeed, as seen in Figure 4b, the excited-state potentials split along ν_{14}, allowing the possibility of singlet−triplet ISC and triplet internal conversion (IC) via the intersection of the corresponding MC PESs.

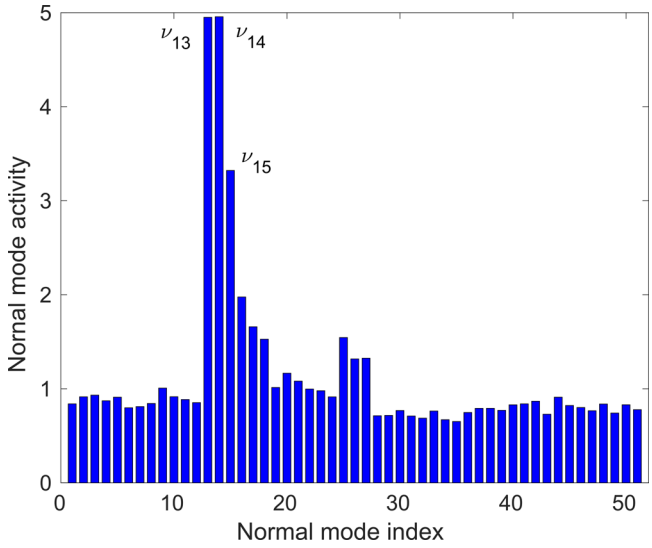

Figure 2. Dynamic normal-mode activity, as determined from the standard deviation of nuclear displacements, projected onto the ground-state normal modes. This was obtained from the singlet−triplet TSH simulations. The labels of the three dominant normal modes, ν_{13}, ν_{14}, and ν_{15}, are depicted. As illustrated in Figure 3, the character of these three modes is Fe−N stretching.

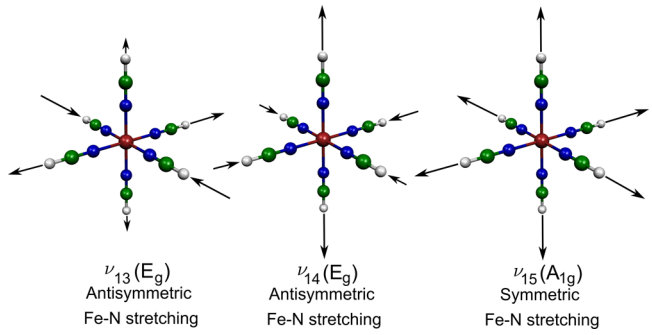

Figure 3. Illustration of the three dominant modes of $[Fe(NCH)_6]^{2+}$, ν_{13} (antisymmetric Fe−N stretching), ν_{14} (antisymmetric Fe−N stretching), and ν_{15} (symmetric Fe−N stretching), identified by the TSH simulations. Also shown are the O_h symmetry labels of the modes.

In Figure 5, we present the electronic population dynamics, as obtained from the three-dimensional QD simulation utilizing the selected modes and all relevant singlet−triplet−quintet states. As shown in the figure, the $^1T_{1g}$ population decay has two components, characterized by the 39 and 168 fs exponential time constants. These time scales are in excellent agreement with the experimentally observed <150 fs ISC.[6] As proposed by Marino et al.,[6] the $^1T_{1g}$ states indeed deactivate via the $^3T_{2g}$ states. Subsequently, the excited-state population flows on a subpicosecond time scale to $^3T_{1g}$ by triplet IC and to the $^5T_{2g}$ manifold via triplet−quintet ISC; as a minor component, the ground state $^1A_{1g}$ is recovered. The $^3T_{1g}$ population is stable on the 1 ps time duration of the simulation, which is consistent with its 39 ps[6] lifetime detected experimentally.[20] Crucially, the simulated dynamics captures all important aspects of the LIESST mechanism revealed by experiments: very fast singlet−triplet ISC, the role of $^3T_{2g}$ states as intermediates, and branching into the HS/LS states. This consistency supports the presented results, which for certain aspects, such as the singlet−triplet ISC, reach even a quantitative agreement with experiment.[6]

https://doi.org/10.1021/acs.inorgchem.1c01838
Inorg. Chem. 2021, 60, 13950−13954

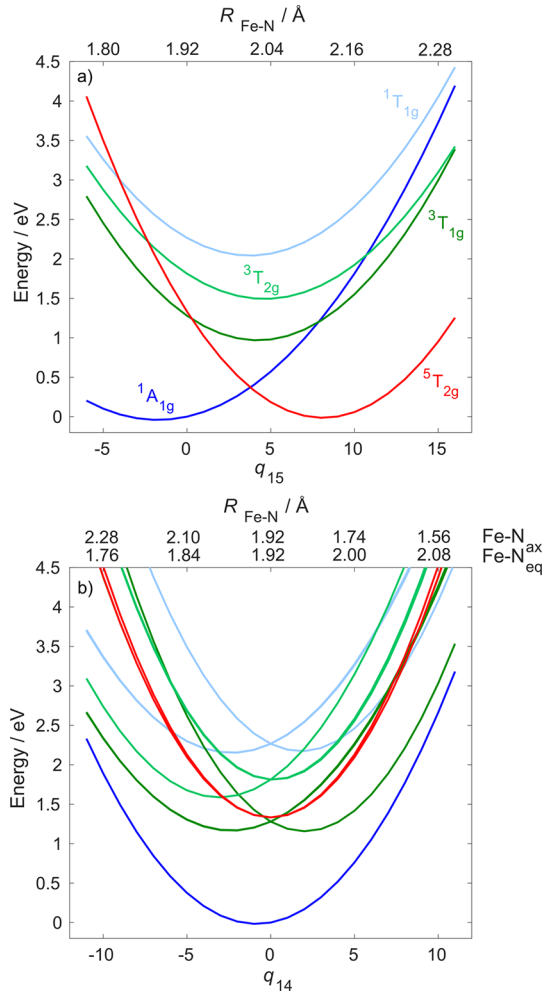

Figure 4. One-dimensional cuts of the diabatic CASPT2 PESs along (a) ν_{15} and (b) ν_{14}. Nuclear displacements are given in dimensionless mass-frequency-scaled normal coordinates and Fe−N distances (Å).

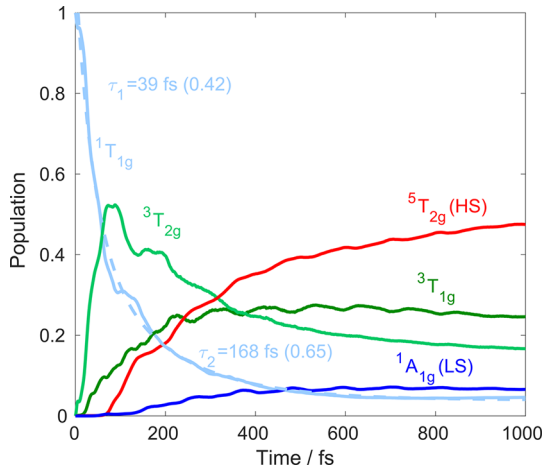

Figure 5. Simulated population dynamics upon excitation into the $^1T_{1g}$ manifold. The $^1T_{1g}$ population curve (light blue) is fitted with a biexponential functional (dashed line); the numbers in parentheses denote the coefficients of the two exponential components.

Finally, we reveal fine details of the LIESST mechanism based on the time evolution of excited-state nuclear wavepackets. We now analyze the singlet−triplet ISC along ν_{14}, which is the natural choice for the involved $^1T_{1g}/^3T_{2g}$ states (occupation of a single e_g* orbital). Figure 6a shows snapshots of the excited-state

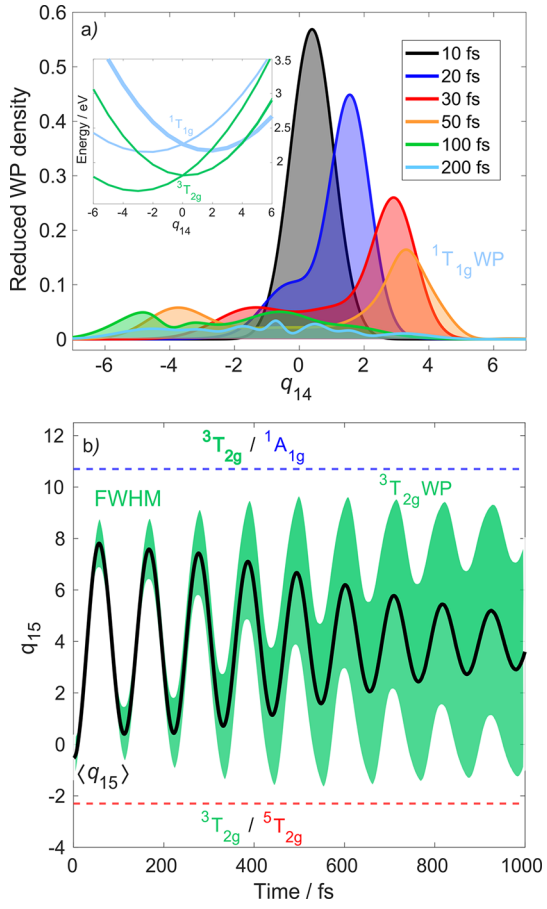

Figure 6. (a) Wavepacket (WP) dynamics along ν_{14} ($^1T_{1g}$ WP). The inset shows the relevant excited-state potentials (the $^1T_{1g}$ component, from which the dynamics is initiated, is displayed using a thick light-blue line). (b) WP dynamics along ν_{15} ($^3T_{2g}$ WP), illustrated by the wavepacket centroid (black) and Gaussian width (green; fwhm). Also shown are the positions of the relevant intersections ($^3T_{2g}/^5T_{2g}$ and $^3T_{2g}/^1A_{1g}$) along ν_{15} (dashed lines).

singlet wavepacket along ν_{14} for the initial 200 fs. The $^1T_{1g}$ wavepacket immediately starts to propagate away from $q_{14} = 0$, entering the $^1T_{1g}/^3T_{2g}$ crossing region. This, combined with a sizable spin−orbit coupling (∼175 and 250 cm^{-1}), allows efficient ISC to the $^3T_{2g}$ manifold, which is indeed what is observed in Figure 5. On the 100−200 fs time scale, the wavepacket becomes more diffuse, which is the reason why the ISC is slower for >100 fs. These results highlight the importance of vibronic motion, as confirmed by the discrepancy between the 36 ps $^1T_{1g} \rightarrow {}^3T_{2g}$ ISC time constant of ref 13 for $[Fe(mtz)_6]^{2+}$, based on Fermi's golden rule, and the <150 fs experimental[6] and simulated 39/168 fs values obtained in this work.

In Figure 6b, we analyze the wavepacket motion in the intermediate $^3T_{2g}$ state along ν_{15}. Clearly, a coherent wavepacket oscillation is induced, with a period of ∼110 fs. The wavepacket dephases and spreads, and, importantly, the Gaussian full width at half-maximum (fwhm, green) does not reach the crossings with the $^5T_{2g}$ and $^1A_{1g}$ states (dashed lines in Figure 6b). This is to say that the $^3T_{2g}$ wavepacket only slightly leaks into the crossing region, which is the reason why the quintet population rises relatively slowly (in $[Fe(bipy)_3]^{2+}$, the HS state is

https://doi.org/10.1021/acs.inorgchem.1c01838
Inorg. Chem. 2021, 60, 13950−13954

populated in <100 fs[7,8]). Although the wavepacket gains more access to the $^3T_{2g}/^5T_{2g}$ intersection along ν_{14}, this channel does not allow significant net population flow to the $^5T_{2g}$ states. This is due to very efficient $^5T_{2g} \rightarrow {}^3T_{1g}$ deactivation, favored by the energetics and easy access to the crossing region (located just at the $^5T_{2g}$ minimum) along ν_{14}, as is clear from Figure 4b.

In this Communication, we revealed the Fe(II) LIESST mechanism of $Fe[(NCH)_6]^{2+}$ using synergistic spin-vibronic dynamics simulations. The obtained mechanistic picture is consistent with the experimental findings and includes assignment of the principal intermediate $^3T_{2g}$, whose dynamics are controlled by the key antisymmetric (ν_{14}) and symmetric (ν_{15}) Fe−N stretching vibrations. Importantly, the present work establishes a new theoretical state of the art for LS → HS photoswitching and will certainly motivate intriguing dynamical studies, both experimental and theoretical ones.

Computational Methods. The TSH simulations are based on Tully's fewest switches,[21] a three-step propagator technique[22] (with transformations between the adiabatic−spin diabatic and diagonal representations), and local diabatization.[23] The QD simulations are based on a diabatic vibronic-coupling[24,25]/spin-vibronic[26−29] Hamiltonian and the multiconfigurational time-dependent Hartree (MCTDH) method.[30] Our methodology uses the following implementations: TSH, *SHARC2.1*[31] interfaced to *ORCA4.2*[32,33] utilizing time-dependent density functional theory (TD-DFT; B3LYP*,[34,35] singlet−triplet states including spin−orbit coupling); QD, Heidelberg *MCTDH8.4*;[30] CASPT2 (12 electrons/14 orbitals: five−five Fe 3d/4d-based, two-σ_{Fe-N} bonding and a pair of Fe 3s/4s correlating active orbitals), *OpenMolcas20.10*.[36] Further details of the utilized methodology are described in the SI.

■ ASSOCIATED CONTENT

Supporting Information

The Supporting Information is available free of charge at https://pubs.acs.org/doi/10.1021/acs.inorgchem.1c01838.

Validity of the $[Fe(NCH)_6]^{2+}$ model, normal-mode frequencies and characters, methodological and computational details of the TSH and QD simulations, and optimized ground-state geometries (PDF)

■ AUTHOR INFORMATION

Corresponding Author

Mátyás Pápai − *Wigner Research Centre for Physics, Budapest H-1525, Hungary;* orcid.org/0000-0002-4819-0611; Email: papai.matyas@wigner.hu

Complete contact information is available at: https://pubs.acs.org/10.1021/acs.inorgchem.1c01838

Notes

The author declares no competing financial interest.

■ ACKNOWLEDGMENTS

The research leading to the presented results has received funding from the Hungarian National Research, Development and Innovation Fund (Grant NKFIH PD 134976). The author acknowledges support from the János Bolyai Scholarship of the Hungarian Academy of Sciences. The author is grateful to Tamás Rozgonyi for fruitful discussions. Guest access to the central HPC cluster of the Technical University of Denmark is acknowledged.

■ REFERENCES

(1) Decurtins, S.; Gütlich, P.; Köhler, C.; Spiering, H.; Hauser, A. Light-induced excited spin state trapping in a transition-metal complex: The hexa-1-propyltetrazole-iron (II) tetrafluoroborate spin-crossover system. *Chem. Phys. Lett.* **1984**, *105*, 1−4.

(2) Létard, J.-F.; Guionneau, P.; Goux-Capes, L. *Spin Crossover in Transition Metal Compounds III*; Springer: Berlin, 2004; pp 221−249.

(3) Bousseksou, A.; Molnár, G.; Matouzenko, G. Switching of Molecular Spin States in Inorganic Complexes by Temperature, Pressure, Magnetic Field and Light: Towards Molecular Devices. *Eur. J. Inorg. Chem.* **2004**, *2004*, 4353−4369.

(4) Cambi, L.; Szegö, L. Über die magnetische Susceptibilität der komplexen Verbindungen. *Ber. Dtsch. Chem. Ges. B* **1931**, *64*, 2591−2598.

(5) Hauser, A. Intersystem crossing in the $[Fe(ptz)_6](BF_4)_2$ spin crossover system (ptz = 1-propyltetrazole). *J. Chem. Phys.* **1991**, *94*, 2741−2748.

(6) Marino, A.; Chakraborty, P.; Servol, M.; Lorenc, M.; Collet, E.; Hauser, A. The Role of Ligand-Field States in the Ultrafast Photophysical Cycle of the Prototypical Iron(II) Spin-Crossover Compound $[Fe(ptz)_6](BF_4)_2$. *Angew. Chem., Int. Ed.* **2014**, *53*, 3863−3867.

(7) Zhang, W.; Alonso-Mori, R.; Bergmann, U.; Bressler, C.; Chollet, M.; Galler, A.; Gawelda, W.; Hadt, R.; Hartsock, R.; Kroll, T.; et al. Tracking excited-state charge and spin dynamics in iron coordination complexes. *Nature* **2014**, *509*, 345−348.

(8) Auböck, G.; Chergui, M. Sub-50-fs photoinduced spin crossover in $[Fe(bpy)_3]^{2+}$. *Nat. Chem.* **2015**, *7*, 629−633.

(9) Moguilevski, A.; Wilke, M.; Grell, G.; Bokarev, S. I.; Aziz, S. G.; Engel, N.; Raheem, A. A.; Kühn, O.; Kiyan, I. Y.; Aziz, E. F. Ultrafast Spin Crossover in $[Fe^{II}(bpy)_3]^{2+}$: Revealing Two Competing Mechanisms by Extreme Ultraviolet Photoemission Spectroscopy. *ChemPhysChem* **2017**, *18*, 465−469.

(10) Vankó, G.; Bordage, A.; Pápai, M.; Haldrup, K.; Glatzel, P.; March, A. M.; Doumy, G.; Britz, A.; Galler, A.; Assefa, T.; et al. Detailed Characterization of a Nanosecond-Lived Excited State: X-ray and Theoretical Investigation of the Quintet State in Photoexcited $[Fe(terpy)_2]^{2+}$. *J. Phys. Chem. C* **2015**, *119*, 5888−5902.

(11) Sousa, C.; Llunell, M.; Domingo, A.; de Graaf, C. Theoretical evidence for the direct ^{3}MLCT-HS deactivation in the light-induced spin crossover of Fe(II)−polypyridyl complexes. *Phys. Chem. Chem. Phys.* **2018**, *20*, 2351−2355.

(12) Sousa, C.; de Graaf, C.; Rudavskyi, A.; Broer, R.; Tatchen, J.; Etinski, M.; Marian, C. M. Ultrafast Deactivation Mechanism of the Excited Singlet in the Light-Induced Spin Crossover of $[Fe(2,2'\text{-bipyridine})_3]^{2+}$. *Chem. - Eur. J.* **2013**, *19*, 17541−17551.

(13) Sousa, C.; de Graaf, C.; Rudavskyi, A.; Broer, R. Theoretical Study of the Light-Induced Spin Crossover Mechanism in $[Fe(mtz)_6]^{2+}$ and $[Fe(phen)_3]^{2+}$. *J. Phys. Chem. A* **2017**, *121*, 9720−9727.

(14) Kepenekian, M.; Robert, V.; Le Guennic, B.; De Graaf, C. Energetics of $[Fe(NCH)_6]^{2+}$ via CASPT2 calculations: A spin-crossover perspective. *J. Comput. Chem.* **2009**, *30*, 2327−2333.

(15) Droghetti, A.; Alfè, D.; Sanvito, S. Assessment of density functional theory for iron(II) molecules across the spin-crossover transition. *J. Chem. Phys.* **2012**, *137*, 124303.

(16) Lawson Daku, L. M.; Aquilante, F.; Robinson, T. W.; Hauser, A. Accurate Spin-State Energetics of Transition Metal Complexes. 1. CCSD(T), CASPT2, and DFT Study of $[M(NCH)_6]^{2+}$ (M = Fe, Co). *J. Chem. Theory Comput.* **2012**, *8*, 4216−4231.

(17) Fumanal, M.; Wagner, L. K.; Sanvito, S.; Droghetti, A. Diffusion Monte Carlo Perspective on the Spin-State Energetics of $[Fe(NCH)_6]^{2+}$. *J. Chem. Theory Comput.* **2016**, *12*, 4233−4241.

(18) Capano, G.; Penfold, T. J.; Chergui, M.; Tavernelli, I. Photophysics of a copper phenanthroline elucidated by trajectory and wavepacket-based quantum dynamics: a synergetic approach. *Phys. Chem. Chem. Phys.* **2017**, *19*, 19590−19600.

(19) Gómez, S.; Heindl, M.; Szabadi, A.; González, L. From Surface Hopping to Quantum Dynamics and Back. Finding Essential Electronic

and Nuclear Degrees of Freedom and Optimal Surface Hopping Parameters. *J. Phys. Chem. A* **2019**, *123*, 8321−8332.
(20) The $^3T_{1g}$ lifetime was measured through the reverse LIESST process, in which the HS state is converted to the LS state by irradiation with 830 nm light.
(21) Tully, J. C. Molecular dynamics with electronic transitions. *J. Chem. Phys.* **1990**, *93*, 1061−1071.
(22) Mai, S.; Marquetand, P.; González, L. A general method to describe intersystem crossing dynamics in trajectory surface hopping. *Int. J. Quantum Chem.* **2015**, *115*, 1215−1231.
(23) Granucci, G.; Persico, M.; Zoccante, A. Including quantum decoherence in surface hopping. *J. Chem. Phys.* **2010**, *133*, 134111.
(24) Cederbaum, L. S.; Köppel, H.; Domcke, W. Multimode vibronic coupling effects in molecules. *Int. J. Quantum Chem.* **1981**, *20*, 251−267.
(25) Köppel, H.; Domcke, W.; Cederbaum, L. S. *Advances in Chemical Physics*; John Wiley & Sons, Ltd., 1984; pp 59−246.
(26) Capano, G.; Chergui, M.; Rothlisberger, U.; Tavernelli, I.; Penfold, T. J. A Quantum Dynamics Study of the Ultrafast Relaxation in a Prototypical Cu(I)−Phenanthroline. *J. Phys. Chem. A* **2014**, *118*, 9861−9869.
(27) Eng, J.; Gourlaouen, C.; Gindensperger, E.; Daniel, C. Spin-Vibronic Quantum Dynamics for Ultrafast Excited-State Processes. *Acc. Chem. Res.* **2015**, *48*, 809−817.
(28) Pápai, M.; Vankó, G.; Rozgonyi, T.; Penfold, T. J. High Efficiency Iron Photosensitiser Explained with Quantum Wavepacket Dynamics. *J. Phys. Chem. Lett.* **2016**, *7*, 2009−2014.
(29) Penfold, T. J.; Gindensperger, E.; Daniel, C.; Marian, C. M. Spin-Vibronic Mechanism for Intersystem Crossing. *Chem. Rev.* **2018**, *118*, 6975−7025.
(30) Beck, M.; Jäckle, A.; Worth, G.; Meyer, H.-D. The multi-configuration time-dependent Hartree (MCTDH) method: a highly efficient algorithm for propagating wavepackets. *Phys. Rep.* **2000**, *324*, 1−105.
(31) Mai, S.; Marquetand, P.; González, L. Nonadiabatic Dynamics: The SHARC Approach. *Wiley Interdiscip. Rev.: Comput. Mol. Sci.* **2018**, *8*, No. e1370.
(32) Neese, F. The ORCA program system. *Wiley Interdiscip. Rev.: Comput. Mol. Sci.* **2012**, *2*, 73−78.
(33) Neese, F. Software update: the ORCA program system, version 4.0. *Wiley Interdiscip. Rev.: Comput. Mol. Sci.* **2018**, *8*, No. e1327.
(34) Reiher, M.; Salomon, O.; Artur Hess, B. Reparameterization of hybrid functionals based on energy differences of states of different multiplicity. *Theor. Chem. Acc.* **2001**, *107*, 48−55.
(35) Reiher, M. Theoretical Study of the $Fe(phen)_2(NCS)_2$ Spin-Crossover Complex with Reparametrized Density Functionals. *Inorg. Chem.* **2002**, *41*, 6928−6935.
(36) Fdez Galván, I.; Vacher, M.; Alavi, A.; Angeli, C.; Aquilante, F.; Autschbach, J.; Bao, J. J.; Bokarev, S. I.; Bogdanov, N. A.; Carlson, R. K.; et al. OpenMolcas: From Source Code to Insight. *J. Chem. Theory Comput.* **2019**, *15*, 5925−5964.

https://doi.org/10.1021/acs.inorgchem.1c01838
Inorg. Chem. 2021, 60, 13950−13954